arXiv:1607.07358v1 [physics.plasm-ph] 25 Jul 2016

Stabilizing effects of resistivity on low-n edge localized modes in NSTX

Debabrata Banerjee and Ping Zhu*

CAS Key Laboratory of Geospace Environment and Department of Modern Physics, University of Science and Technology of China, Hefei, Anhui 230026, China and Department of Engineering Physics, University of Wisconsin-Madison, Madison, Wisconsin 53706, USA

Rajesh Maingi

Princeton Plasma Physics Laboratory, P.O. Box 451*, Princeton, New Jersey 08543, USA*

(Dated: July 26, 2016)

Abstract

The stabilizing effects of enhanced edge resistivity on the low-n edge localized modes (ELMs) are reported for the first time in the context of ELM suppression in H-mode discharge due to lithium-conditioning in the National Spherical Torus Experiment (NSTX). Here n is the toroidal mode number. Linear stability analysis of the corresponding experimental equilibrium suggests that the change in the equilibrium plasma density profile alone due to lithium-conditioning may be insufficient for a complete suppression of ELMs. The enhanced resistivity due to the increased effective electric charge number $Z_{\rm eff}$ after lithium-conditioning can account for additional stabilization effects that contribute to robust ELM suppression. Remarkably, such a stabilizing effect of enhanced edge resistivity on the low-n ELMs only exists when two-fluid effects are considered in the MHD model.

The edge localized mode (ELM) has been a primary concern to the next generation of long-pulse, steady-state burning plasma experiments such as ITER [1, 2] and CFETR [3]. This is because ELMs play a central role in the periodic loss of particles and power from the collapse of edge pedestal in the high confinement regime, i.e. H-mode of tokamaks [4–6]. Apart from the deterioration in plasma confinement, they cause physical damage to divertor plates and other plasma facing components through repetitive heat loads and particle deposition [7]. One of the effective ELM suppression and mitigation method has been the injection of low-z impurity particles (e.g, lithium) into tokamak during or immediately prior to the discharge [8–10]. This method was first successfully applied in NSTX through lithium coated divertor plates and ELM-free H-mode discharges have been achieved [9, 11]. Then, combined techniques of real time lithium-injection and prior discharge lithium-coating has been effectively applied to the Experimental Advanced Superconducting Tokamak (EAST) to produce 20 sec long ELM-free H-mode discharge [8]. More detailed understanding of this method is desirable in order to design its effective implementation towards controlling ELMs in ITER.

A systematic study of H-mode discharge with decreasing ELM frequency and amplitude has been carried out in NSTX after gradually increasing the thickness of lithium coatings on wall and divertor plates [12, 13]. Lithium conditioning reduces plasma recycling which in turn helps to minimize core fueling from divertor recycling sources and thus the edge electron density in the scrape-off layer and the near-separatrix region are reduced. This process eventually moves inward the pedestal positions of electron density and temperature profiles away from separatrix and the profiles become widen in comparison to the pre-lithium discharges. Besides those profile modifications, toroidal rotation and effective atomic number ($Z_{\rm eff}$) substantially increase after lithium conditioning of plasma facing components, especially after ELM elimination. A series of recent reports from NSTX has documented in details of the effect and outcome of lithium-conditioning, including its potential relation to ELM-free H-mode. This letter presents a new explanation on the additional impurity induced stabilization of NSTX ELM-free discharge based on our independent findings of stabilizing effect of resistivity on the low-n edge localized modes [14, 15].

The equilibrium of NSTX ELMy discharge is predicted to be close to the kink/peeling unstable boundary from the analysis using the ideal magnetohydrodynamic (MHD) code ELITE with inclusion of the stabilizing effects from the diamagnetic drift and the finite

Larmor radius. Following the same analysis, the post-lithium ELM-free case is found to be within the stable regime of the peeling-ballooning instability diagram. It is argued that due to the inward shift of the edge peak pressure gradient to a lower magnetic shear region and substantial decrease of pedestal pressure gradient, the ballooning components have become stable. The reduced profile peaking of the edge bootstrap current density has enabled the peeling components to become stable. Those arguments led to earlier conclusion that the whole stabilization scenario is mainly the consequence of equilibrium profile modification due to lithium-conditioning.

This present letter contains the linear stability analysis results from the first-principle based initial value extended MHD code NIMROD [16], which has been benchmarked and verified for the analysis of both ideal and non-ideal physical processes [17–24]. The equilibriums we study are from the pre-lithium reference ELMy H-mode (#129015) discharge and the post-lithium ELM-free H-mode (#129038) discharge from NSTX experiments [9] (Fig. 1). The purpose of our analysis is to crosscheck the cause behind the stabilization of ELMs, including the ideal MHD effects from the equilibrium profile modifications and the non-ideal MHD effects due to the increase of resistivity through $Z_{\rm eff}$ enhancement in the post-lithium discharge. The change in resistivity is not the only consequence of the $Z_{\rm eff}$ enhancement. In particular, changing $Z_{\rm eff}$ can significantly change the bootstrap current profile. Since the experimental equilibrium profiles are used in our analysis, all profile changes, including those of plasma current from changing $Z_{\rm eff}$, have been fully taken into account in our calculations. Our findings suggest that the previous explanation on the ELM suppression after lithium conditioning based purely on the profile modification may be incomplete. The main new result of this letter is that the enhancement of resistivity due to the increase of $Z_{\rm eff}$ after lithium usage, can play a direct and crucial role towards ELM stabilization, in addition to the effects from pedestal profile modifications.

The remainder of this letter is organized as follows. First, the main results of stabilization of the low-n peeling-ballooning modes by enhanced resistivity with increase of $Z_{\rm eff}$ is described. Here n is the toroidal mode number. Second, the convergence test with different crucial numerical parameters of simulation has been detailed. Third, similar stability analysis on the pre-lithium ELMy case has been shown, with clear indication of stabilizing effects of resistivity on the low-n edge modes. Finally, conclusion is drawn along with discussions on the probable physical explanation.

The extended MHD equations used in our NIMROD calculations are:

$$\frac{\partial n}{\partial t} + \nabla \cdot (n\mathbf{u}) = 0 \tag{1}$$

$$mn\left(\frac{\partial}{\partial t} + \mathbf{u}\cdot\nabla\right)\mathbf{u} = \mathbf{J}\times\mathbf{B} - \nabla p - \nabla\cdot\overline{\Pi} \tag{2}$$

$$\frac{3}{2}\left(\frac{\partial}{\partial t} + \mathbf{u}_\alpha\cdot\nabla\right)T_\alpha = -nT_\alpha\nabla\cdot\mathbf{u}_\alpha - \nabla\cdot\mathbf{q}_\alpha \qquad (\alpha = i, e) \tag{3}$$

$$\frac{\partial \mathbf{B}}{\partial t} = -\nabla\times\left[\eta\mathbf{J} - \mathbf{u}\times\mathbf{B} + \frac{1}{ne}\left(\mathbf{J}\times\mathbf{B} - \nabla p_e\right)\right] \tag{4}$$

$$\mu_0\mathbf{J} = \nabla\times\mathbf{B}; \qquad \nabla\cdot\mathbf{B} = 0 \tag{5}$$

where $\mathbf{u}$ is the center-of-mass flow velocity with particle density n and ion mass m, p is the combined pressure of electron (p_e) and ion (p_i), η represents resistivity, $\mathbf{q}_{e,i}$ denote conductive heat flux vectors and $\overline{\Pi}$ is ion stress tensor including gyro-viscous components as described in the earlier reference [17].

In our analysis of the post-lithium case (#129038) using NIMROD, all toroidal modes in the range $n = 1 - 10$ are found to be stable in the ideal two-fluid MHD limit, except the modes with $n = 3, 4$. Modes above $n = 4$ are stabilized after including the two-fluid diamagnetic drift and the finite Larmor radius (FLR) stabilization effects. Modes $n = 1, 2$ are stabilized even in the MHD scenario itself. The left panel of Fig. 2 shows the two-fluid effects in comparison to the ideal MHD model. These results are consistent with NSTX ELMy discharge experiments where the low-n modes are the dominant components in the ELM precursor signals measured from divertor. Spitzer resistivity model ($\eta(T_e) = \eta_0 Z_{\rm eff}(T_{e0}/T_e)^{3/2}$) is adopted in the calculation, where T_{e0}, $\eta_0 Z_{\rm eff}$, T_e denote electron temperature, resistivity at the magnetic axis, and the electron temperature profile, respectively. The effect of gyro-viscosity is also included in the 2-fluid calculations. The whole simulation domain is divided into a plasma region and a vacuum region with the real wall configuration of NSTX. The vacuum in these calculations is modeled using the low temperature, low density and high resistivity plasma in what is often referred to as halo region. The values of these parameters in vacuum are naturally determined by the experimental profiles for both pre- and post-lithium discharges used in our calculations. A scanning of the resistivity value through changing $Z_{\rm eff}$ reveals that the growth rates of $n = 3$ and $n = 4$ modes decrease with increasing η, as shown in the right panel of Fig. 2. Such a scanning is motivated by the experiment where $Z_{\rm eff}$ is enhanced substantially by carbon accumulation as ELMs disappear [25]. The contour plots of the $n = 3, 4$ modes shown in Figs. 3 and 4 bear the signature of the characteristics

of edge localized modes. The stabilization of the $n = 3, 4$ modes with enhanced resistivity in the two-fluid MHD model has not been reported elsewhere. A thorough test verifying the convergence of above results has been done with respect to time step, azimuthal grid points, and other numerical parameters (Fig. 5).

It is worth mentioning that this resistive effect on the low-n edge localized modes is feasible only with the inclusion of the two-fluid effects in the MHD model. For purely resistive MHD model without inclusion of 2-fluid effects, the increase in resistivity always destabilizes all range of the edge localized modes. This contrasts to the recent study using NIMROD where the resistive stabilizing effects on low-n edge localized modes appear in both the single-fluid and the two-fluid MHD models [24] which might be arising from different resistivity model used in ideal and resistive limit. Our results also differs from resisitive effect studies on peeling-ballooning modes in other codes as M3D-C^1 (in single fluid limit [26]) and BOUT++ (in 2-fluid limit with constant resistivity profile [27]). Thus the results regarding the effect of edge resistivity on low-n peeling-ballooning modes in a 2-fluid MHD model have not been reported in the literature, to our knowledge. To check if such an effect also exists for pre-lithium ELMy H-mode discharge, we have analyzed one of these cases thoroughly using NIMROD. First, comparison between full resistive MHD and extended MHD model shows increase of growth rate for $n = 3, 4$ modes and reduction of growth rate for other higher n modes (Left panel of Fig. 6). This result is consistent with experimental observation and previous eigenvalue code prediction of growing low-n modes. A scanning of Z_{eff} through the resistivity model has been done artificially to evaluate possible resistive effects on the edge localized modes for the pre-lithium equilibrium configuration. The results in the Fig. 6 shows that increase of resistivity has opposite effects for low-n ($n = 3 - 6$) and high-n (after $n = 6$) modes. That is, the low-n modes are stabilized with the increase of Z_{eff} up to 4. However, high-n modes become more unstable with the increase of resistivity. But, for the post-lithium case (Fig. 2), modes higher than $n = 4$ remain stable even after the increase of resistivity.

In summary, the resistive effect towards stabilization of the low-n edge localized modes only from a 2-fluid MHD model is reported, and such an effect has been applied as a new explanation to the observed ELM suppression after lithium conditioning in NSTX for the first time. The conclusion is based on our stability analysis of the lithium-conditioned ELM-free H-mode experimental profiles from NSTX using the initial value MHD code NIMROD.

For the post-lithium pedestal profiles, the profile improvement has been found responsible for suppressing higher-n ($n > 4$) modes. However, the $n = 3, 4$ modes are found to remain unstable with edge localized mode structure even in the ideal 2-fluid MHD model. The finding differs from the earlier eigenvalue-code based analysis and explanation on the probable mechanism behind the observed suppression of ELMs in the NSTX experiment [9, 13]. When the enhanced resistivity due to the substantial increase of Z_{eff} observed in experiment is taken into account, the remaining unstable $n = 4$ mode can be fully stabilized along with partial stabilization of $n = 3$. This result shows a clear trend of low-n mode stabilization with higher Z_{eff}. Unlike the destabilizing effect of resistivity on all range of peeling-ballooning modes in the single-fluid MHD model, the stabilizing effect of resistivity on the low-n edge localized mode is only obtainable from the two-fluid MHD model. Such a newly found resistive stabilizing effect may contribute to the complete physical mechanism behind the lithium-induced ELM suppression through a virtuous cycle – the initial refinement in electron pressure profile after the reduction in divertor recycling leads to the initial reduction of ELM frequency and size, with the consequence of increasing Z_{eff} due to impurity accumulation at edge pedestal. The enhancement in Z_{eff} brings in the additional resistive stabilization of the low-n ELMs, which would in turn reinforce the impurity accumulation and the resulting Z_{eff} enhancement until the complete ELM suppression.

To further establish the universality of the effects reported here, more analyses need to be performed for other lithium-conditioned ELM experiments such as those in EAST as well, where the enhancement in Z_{eff} and collisionality are observed in the post-lithium discharge [8]. These may render more detailed understanding of this newly discovered physics, and help further design and implement lithium delivery methods for controlling ELMs in future fusion devices.

The research was supported by the National Magnetic Confinement Fusion Program of China under Grant Nos. 2014GB124002, 2015GB101004, and the 100 Talent Program of the Chinese Academy of Sciences (CAS). Author D. B. is partially supported by CAS President International Fellowship Initiative (PIFI). We are grateful for the discussions with Charlson C. Kim, the help from Shikui Cheng, and the support from the NIMROD team. This research used resources of the National Energy Research Scientific Computing Center, a DOE Office of Science User Facility supported by the Office of Science of the U.S. Department of Energy under Contract No. DE-AC02-05CH11231. The experiment in NSTX was supported by

DOE under Contract No. DE-AC02-09CH11466. The digital data for this paper is available at http://arks.princeton.edu/ark:/88435/dsp01vx021h49j.

* pzhu@ustc.edu.cn

[1] A. Loarte, B. Lipschultz, and A. S. Kukushkin et. al., Nucl. Fusion **47**, S203 (2007).

[2] P. T. Lang, A. Loarte, and G. Saibene et. al., Nucl. Fusion **53**, 043004 (2013).

[3] V. S. Chan, A. Costley, and B.N. Wan et. al., Nucl. Fusion **55**, 023017 (2015).

[4] F. Wagner, G. Becker, and K. Behringer et. al., Phys. Rev. Lett. **49**, 1408 (1982).

[5] H. Zohm, Plasma Phys. Control. Fusion **38**, 105 (1996).

[6] J. W. Connor, Plasma Phys. Control. Fusion **40**, 191 (1998).

[7] G. Federici, P. Andrew, and P. Barabaschi,et. al., J. Nucl. Matter **313**, 11 (2003).

[8] J. S. Hu, Z. Sun, and H. Y. Guo et. al., Phys. Rev. Lett. **114**, 055001 (2015).

[9] R. Maingi, T. H. Osborne, and B. P. LeBlancet. al., Phys. Rev. Lett. **103**, 075001 (2009).

[10] T. H. Osborne, G. L. Jackson, and Z. Yan et. al., Nucl. Fusion **55**, 063018 (2015).

[11] R. Maingi, S. M. Kaye, and C. H. Skinner et. al., Phys. Rev. Lett. **107**, 145004 (2011).

[12] R. Maingi, D. P. Boyle, and J.M. Canik et al., Nucl. Fusion **52**, 083001 (2012).

[13] D. P. Boyle, H. W. Kugel, and R Kaita et. al., Plasma Phys. Control. Fusion **53**, 105011 (2011).

[14] D. Banerjee (2016), presentation in 29th ITPA Pedestal Edge Physics Group March meeting.

[15] H. Urano (2016), 29th ITPA Pedestal Edge Physics Group meeting summary.

[16] C. R. Sovinec, A. Glasser, and the NIMROD Team, J. Comp. Phys. **195**, 355 (2004).

[17] C. R. Sovinec, J. R. King, and the NIMROD Team, J. Comp. Phys. **229**, 5803 (2010).

[18] D. P. Brennan, S. E. Kruger, and D. D. Schnack et. al., J. Phys. : Conf. Series **46**, 63 (2006).

[19] P. Zhu and J. Raeder, Phys. Rev. Lett. **110**, 235005 (2013).

[20] B. J. Burke, S. E. Kruger, and C. C. Hegna et. al., Phys. Plasmas **17**, 032103 (2010).

[21] F. Ebrahimi and R. Raman, Phys. Rev. Lett. **114**, 205003 (2015).

[22] V. A. Izzo, P. Parks, and N. W. Eidietis et al., Nucl. Fusion **55**, 073032 (2015).

[23] P. Zhu, D. D. Schnack, and F. Ebrahimi et. al., Phys. Rev. Lett. **101**, 085005 (2008).

[24] J. R. King, A. Y. Pankin, and S. E. Kruger et. al., Phys. Plasmas **23**, 062123 (2016).

[25] F. Scotti, V. Soukhanovskii, and R.E. Bell et. al., Nucl. Fusion **53**, 083001 (2013).

[26] N. M. Ferraro, S. C. Jardin, and P. B. Snyder, Phys. Plasmas **17**, 102508 (2010).

[27] B. D. Dudson, X. Q. Xu, and M. V. Umansky et. al., Plasma Phys. Control. Fusion **53**, 054005 (2011).

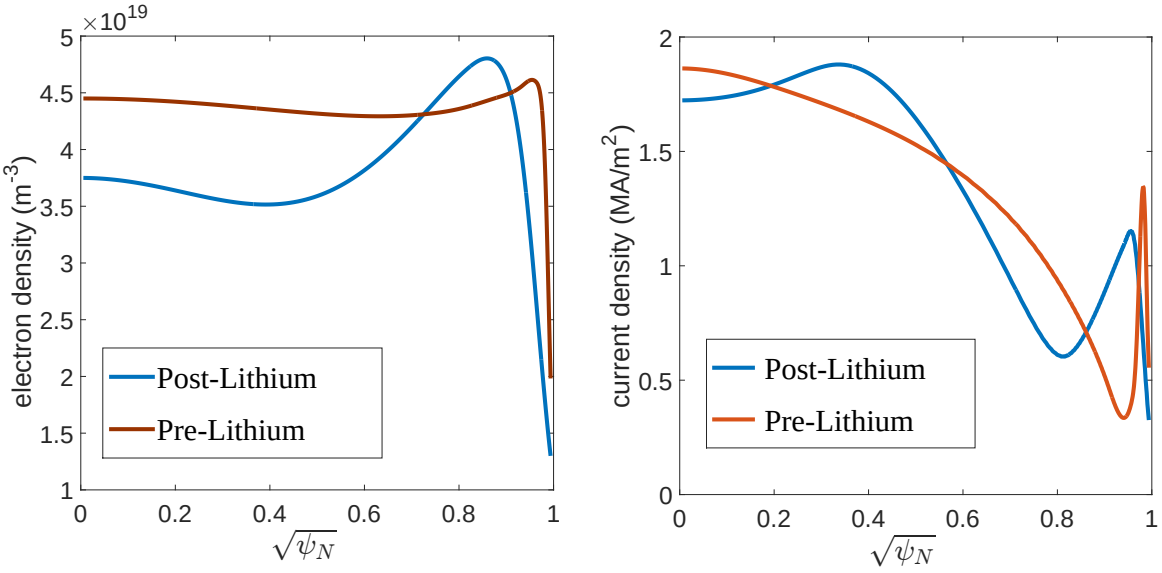

FIG. 1: Electron density (left) and current density (right) radial profiles of NSTX ELM experiments. Blue solid lines correspond to post-lithium discharge and red dotted lines to the pre-lithium reference discharge. ψ_N is the normalized poloidal flux function.

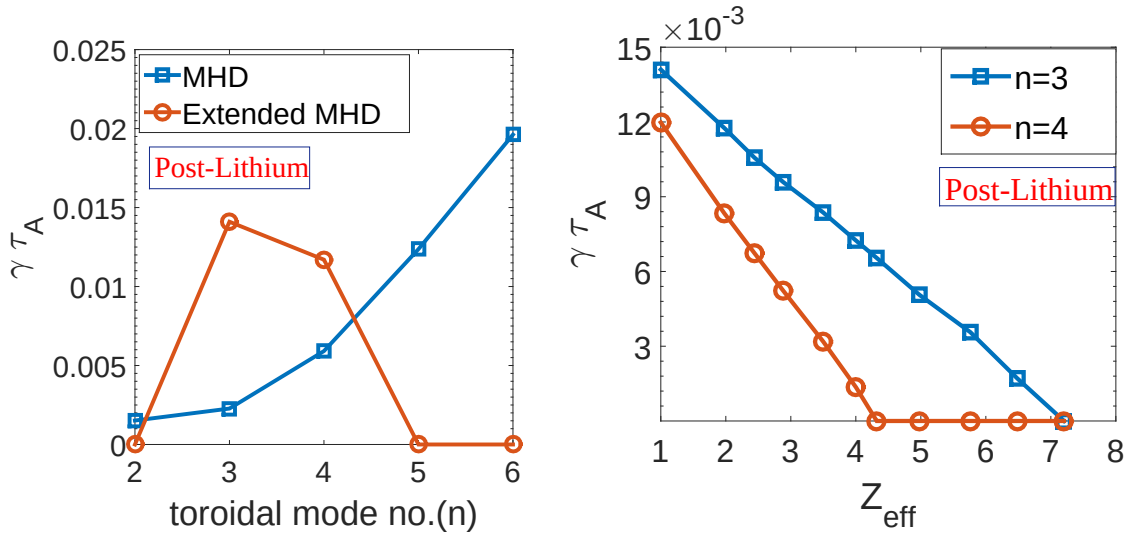

FIG. 2: (Post-Lithium discharge #129038) Left: Linear growth rates as function of toroidal mode number from resistive MHD (blue circled curve) and extended MHD (red squared curve) calculations respectively using NIMROD for the post-lithium case. Right: Linear growth rates of $n = 3, 4$ modes as function of $Z_{\rm eff}$. Experimentally measured $Z_{\rm eff}$ at the edge ranges between 3.5 (at $\psi_N = 0.9$) and 4.0 at ($\psi_N = 0.7$) in the post-lithium discharge (see Fig. 2 of Ref. [12]).

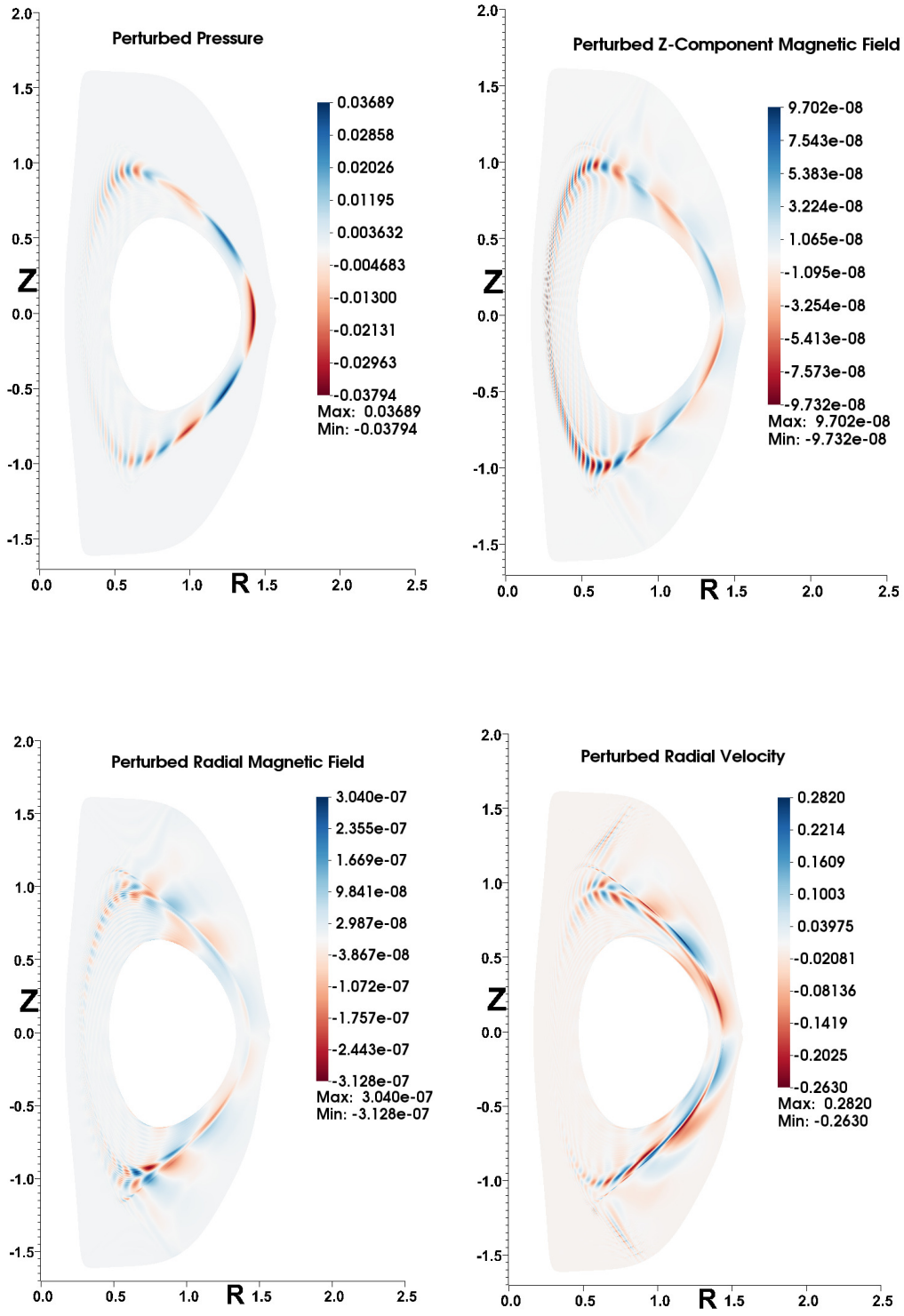

FIG. 3: Contour plots of perturbed quantities pressure, B_z, B_r and u_r for $n = 4$ mode for the post-lithium case.

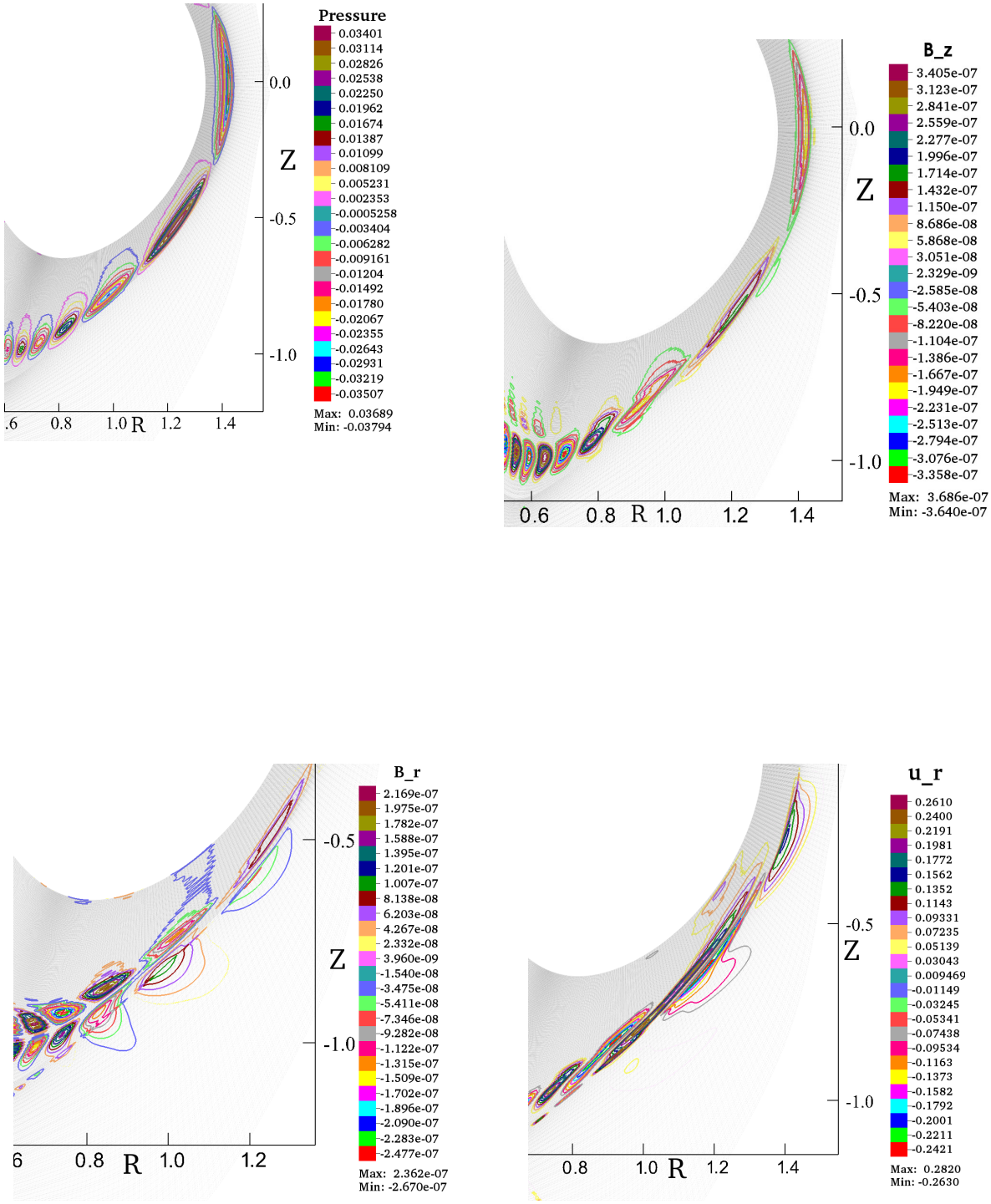

FIG. 4: Zoomed-in contour plots of perturbed quantities pressure, B_z, B_r and u_r for $n = 4$ mode for the post-lithium case, showing detailed mode structure.

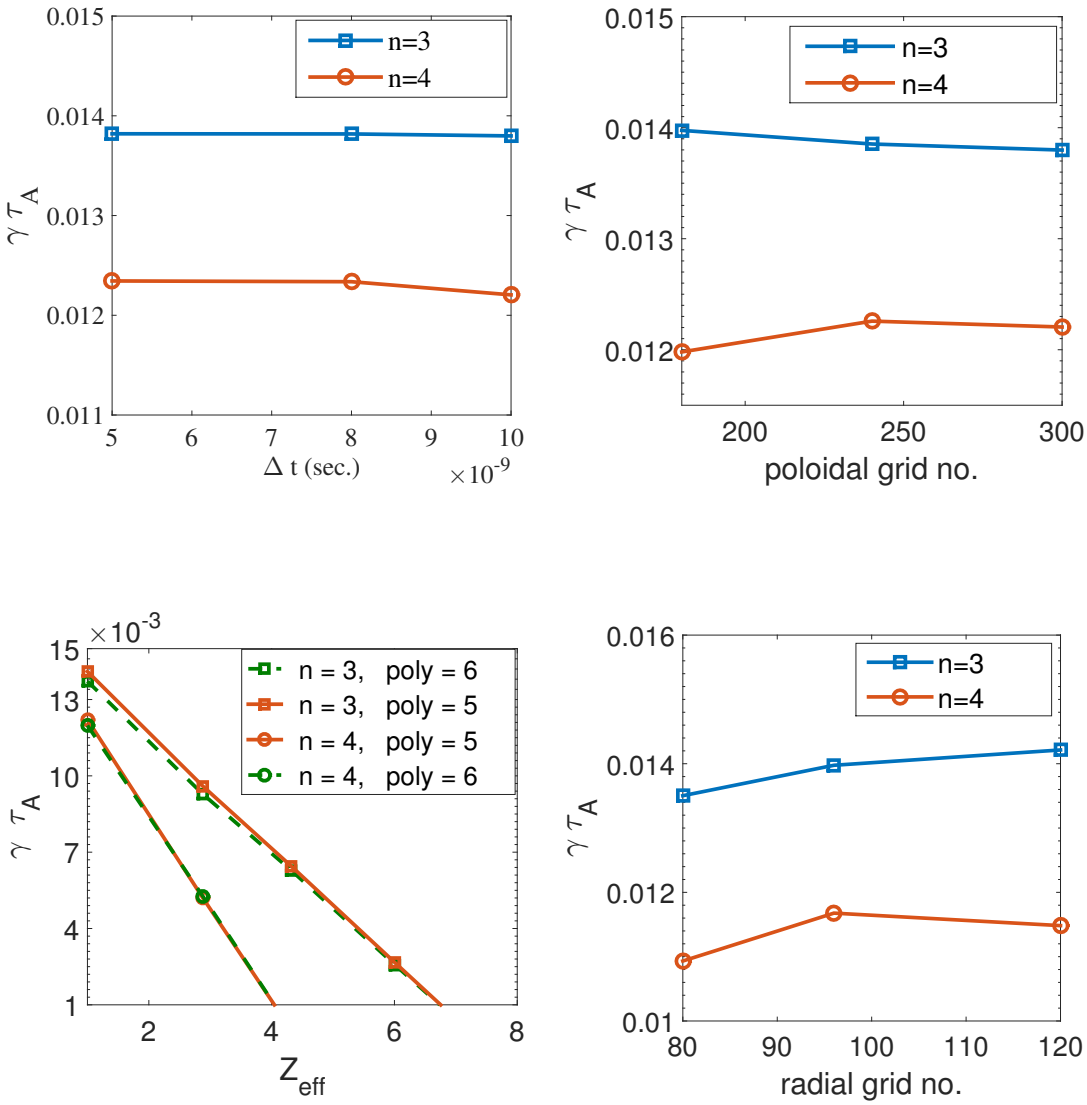

FIG. 5: (Post-Lithium discharge #129038) Linear growth rates for $n = 3, 4$ modes as function of numerical parameters such as time step, numbers of grid points in azimuthal direction and radial direction, polynomial degree of finite elements used in NIMROD calculations.

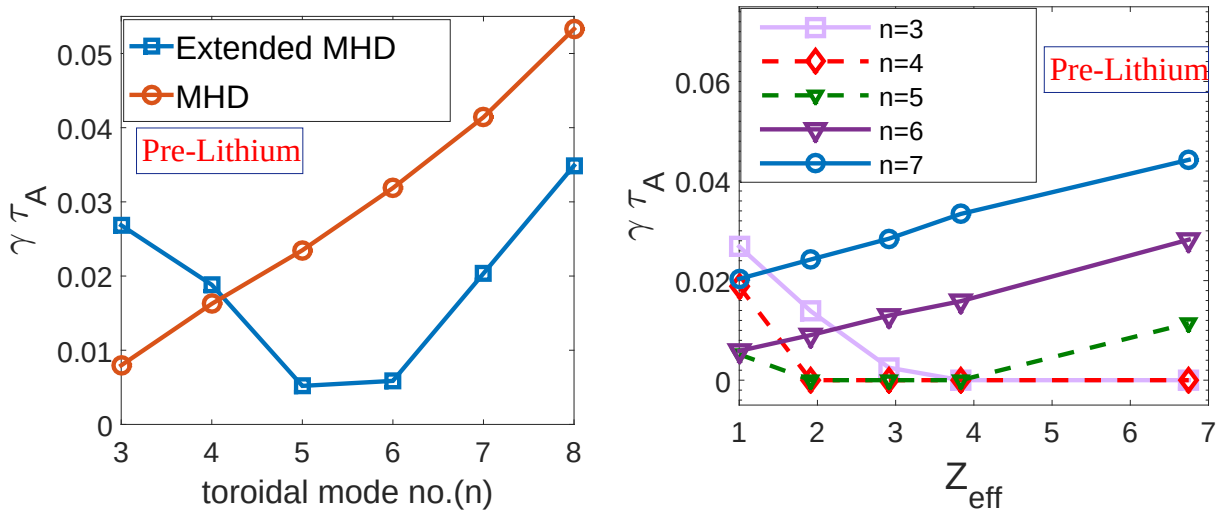

FIG. 6: (Pre-Lithium discharge #129015) Left: Linear growth rates as function of toroidal mode number from resistive MHD (blue circled curve) and extended MHD (red squared curve) calculations respectively using NIMROD for the pre-lithium case. Right: Linear growth rates of $n = 3, 4$ modes as function of Z_{eff}. Experimentally measured Z_{eff} at the edge ranges between 2.0 (at $\psi_N = 0.7$) and 2.2 (at $\psi_N = 0.9$) in the pre-lithium discharge.